Research
Green Chemical Engineering—Article

Effects of Potassium and Manganese Promoters on Nitrogen-Doped Carbon Nanotube-Supported Iron Catalysts for CO_2 Hydrogenation

Praewpilin Kangvansura[a], Ly May Chew[b], Chanapa Kongmark[c], Phatchada Santawaja[d], Holger Ruland[b], Wei Xia[b], Hans Schulz[e], Attera Worayingyong[c], Martin Muhler[b,*]

[a] *Scientific Equipment Center, Faculty of Science, Kasetsart University, Bangkok 10900, Thailand*
[b] *Laboratory of Industrial Chemistry, Ruhr-University Bochum, Bochum 44780, Germany*
[c] *Department of Materials Science, Faculty of Science, Kasetsart University, Bangkok 10900, Thailand*
[d] *Department of Chemistry, Faculty of Science, Kasetsart University, Bangkok 10900, Thailand*
[e] *Engler-Bunte-Institute, Karlsruhe Institute of Technology, Karlsruhe 76131, Germany*
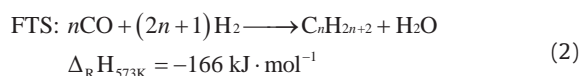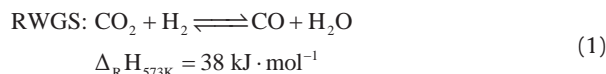
ARTICLE INFO

ABSTRACT

Nitrogen-doped carbon nanotubes (NCNTs) were used as a support for iron (Fe) nanoparticles applied in carbon dioxide (CO_2) hydrogenation at 633 K and 25 bar (1 bar = 10^5 Pa). The Fe/NCNT catalyst promoted with both potassium (K) and manganese (Mn) showed high performance in CO_2 hydrogenation, reaching 34.9% conversion with a gas hourly space velocity (GHSV) of 3.1 L·(g·h)$^{-1}$. Product selectivities were high for olefin products and low for short-chain alkanes for the K-promoted catalysts. When Fe/NCNT catalyst was promoted with both K and Mn, the catalytic activity was stable for 60 h of reaction time. The structural effect of the Mn promoter was demonstrated by X-ray diffraction (XRD), temperature-programmed reduction (TPR) with molecular hydrogen (H_2), and *in situ* X-ray absorption near-edge structure (XANES) analysis. The Mn promoter stabilized wüstite (FeO) as an intermediate and lowered the TPR onset temperature. Catalytic ammonia (NH_3) decomposition was used as an additional probe reaction for characterizing the promoter effects. The Fe/NCNT catalyst promoted with both K and Mn had the highest catalytic activity, and the Mn-promoted Fe/NCNT catalysts had the highest thermal stability under reducing conditions.

1. Introduction

Emission of the primary greenhouse gas, carbon dioxide (CO_2), from human activities has continuously risen in recent years. Hydrogenation of CO_2 is considered to be an alternative route for converting it to valuable chemicals and fuel. It is generally accepted that the hydrogenation process occurs in two consecutive reactions: the reverse water gas shift (RWGS) reaction, followed by the Fischer-Tropsch synthesis (FTS), as described in Eqs. (1) and (2) [1,2]:

$$\text{RWGS: } CO_2 + H_2 \rightleftharpoons CO + H_2O$$
$$\Delta_R H_{573K} = 38 \text{ kJ} \cdot \text{mol}^{-1} \tag{1}$$

$$\text{FTS: } nCO + (2n+1)H_2 \longrightarrow C_nH_{2n+2} + H_2O$$
$$\Delta_R H_{573K} = -166 \text{ kJ} \cdot \text{mol}^{-1} \tag{2}$$

The reaction of molecular hydrogen (H_2) and CO_2 to produce water (H_2O) and carbon monoxide (CO) is the RWGS reaction, which is industrially catalyzed by magnetite (Fe_3O_4). CO, which is produced as the reactant gas for the FTS reaction, is catalytically converted in the presence of H_2 into hydrocarbons through a surface hydrogenation-polymerization reaction. FTS is catalyzed by metals such as cobalt (Co), iron (Fe), or ruthenium (Ru). Fe catalysts have been a favored choice in CO_2 hydrogenation because they are readily available and have a high RWGS activity, producing olefins and branched hydrocarbons. Co catalysts are not suitable for CO_2 hydrogenation, even with added RWGS promoters such as manganese (Mn) and potassium (K), because the partial pressure of the CO produced is too low [3–5].

Riedel et al. [6] found that the trends of catalytic activity and selectivity in both processes were almost the same when using K-promoted Fe catalysts for CO/H_2 and CO_2/H_2 synthesis. The duration

of different kinetic regimes was longer when using CO_2/H_2 than when using CO/H_2. Their product selectivity results indicated that the CO_2 hydrogenation reaction occurs together with CO hydrogenation (FTS reaction) [7,8]. They also reported that iron carbide (Fe_3C) formed on the Fe catalyst surface via CO produced from the RWGS reaction [6]. For Fe catalysts, the formation of surface carbides is required before the catalyst can exhibit Fischer-Tropsch (FT) activity [4,9–15]. Potassium is assumed to enhance basicity and to inhibit H_2 dissociative adsorption [6,7,16,17]. In this way, it increases olefin selectivity and chain-growth probability, suppresses methane formation, and improves iron carbide formation [15,18,19]. Nevertheless, carbon deposition on the iron carbide phase induces catalyst deactivation. Manganese acts as a structural and electronic promoter, enhancing the dispersion of iron oxide on the surface and suppressing reduction and carburization of the catalyst in the syngas reduction process. As a result, it decreases the deactivation rate of Fe catalysts under FTS reaction conditions [20–22]. Davis [23] proposed that an oxygen-containing structure as a formate species could form from either CO or CO_2 for chain initiation. Under reaction conditions, the catalyst consists of a core of Fe_3O_4, which is covered by a layer of iron carbide. During the reaction, the layer of iron carbide must be maintained.

Carbon nanotubes (CNTs) are promising support materials [24–27] due to their large surface area and their ability to disperse catalytically active nanoparticles [28]. They also prevent sintering, thus improving the stability and activity of Fe FTS catalysts [8,17]. Oxygen- and nitrogen-containing functional groups in CNTs are assumed to act as coordination sites for metal active species [24,25]. Nitrogen-doped CNTs (NCNTs) can be obtained by the post-treatment of partially oxidized CNTs (OCNTs) in flowing ammonia (NH_3) [24,29]. Kundu et al. [29] found that after an NH_3 treatment at 673 K, NCNTs contain mainly pyridinic groups, which are considered to be coordination sites for active metal species. A mixture of 49% wüstite (FeO) and 51% metallic iron was observed by Chew et al. [2] after 5 h at 753 K. Fe/NCNT, Fe/OCNT, and Fe/SiO_2 were used for CO_2 hydrogenation, with Fe/NCNT having a lower CO selectivity than Fe/OCNT. Fe/SiO_2 was found to be much less suitable for CO_2 hydrogenation compared with the CNT-supported catalysts. The C_1–C_5 hydrocarbon selectivities that were obtained with Fe/NCNT were clearly higher than those obtained with Fe/OCNT. Based on the proposed CO_2 hydrogenation reaction step, CO produced from the RWGS reaction is hydrogenated to hydrocarbons. Chew et al. [2] concluded that the hydrogenation of CO on Fe/NCNT was faster than the reaction on Fe/OCNT, and that all catalysts after the reaction were in the carbided state.

The decomposition of NH_3 is a reaction that is catalyzed by many transition metal surfaces [30,31]. Recombinative desorption of chemisorbed atomic nitrogen is the rate-determining step in NH_3 decomposition [30]. Thus, NH_3 decomposition was used to characterize the effects of promoters on the thermal stability of the reduced catalysts.

This study focuses on the effect of K and Mn on the activity, product selectivity, and thermal stability of NCNT-supported Fe catalysts. Iron nanoparticles supported on NCNTs were synthesized via impregnation. Phase analysis was performed by X-ray diffraction (XRD). Temperature-programmed reduction with H_2 (H_2-TPR) and in situ X-ray absorption near-edge structure (XANES) analysis were used to investigate the reducibility of the Fe catalysts. NH_3 decomposition and CO_2 hydrogenation over K/Mn-promoted iron nanoparticles supported on NCNTs were applied to assess the catalytic performance of the Fe catalysts and to probe the promoter effects. A recent study focused on the influence of the promotors on the product distribution [32].

2. Experimental section

2.1. Catalyst preparation

The Fe catalysts were synthesized by the impregnation of NCNTs using ammonium ferric citrate ($C_6H_8O_7 \cdot x Fe^{3+} \cdot y NH_3$) as an Fe precursor [29,33,34] followed by impregnation with aqueous solutions of manganese (II) nitrate hydrate ($Mn(NO_3)_2 \cdot x H_2O$) and potassium carbonate (K_2CO_3) to obtain the K- and Mn-promoted Fe catalyst (K/Mn/Fe/NCNT), as described in detail in Ref. [32].

2.2. Characterization

The actual catalyst compositions were determined quantitatively using atomic absorption spectrometry (AAS). XRD was performed to determine the crystalline phases present in the catalysts using a diffractometer (PANalytical; X'Pert PRO MPD) with Cu Kα radiation (λ = 1.54 Å) and an electron current of 40 mA with an accelerating voltage of 45 kV. The spectra were scanned with a step size of 0.026° in the 2θ range of 20°–80°. The identification of crystalline phases was accomplished using the inorganic crystal structure database (ICSD). H_2-TPR was performed by heating 40 mg of catalyst with a heating rate of 10 K·min⁻¹ in a mixture gas of 4.73% H_2 in argon (Ar) with a flow rate of 84.1 cm³·min⁻¹. The sample was heated from 323 K to 1073 K and held at that temperature for 1 h.

The reduction behavior of the catalysts was monitored using in situ XANES analysis under a hydrogen atmosphere at the time-resolved X-ray absorption spectroscopy (XAS) beamline (BL2.2) of the Synchrotron Light Research Institute (SLRI) in Thailand. A bent crystal Si(111) in the energy-dispersive monochromator was used to focus a polychromatic X-ray beam onto the sample [35]. The X-rays pass through the sample and then diverge toward a position-sensitive detector (an NMOS-linear image sensor), with a data collection time of 250 ms. Samples of 4.5 mg were prepared as 4 mm diameter pellets. In situ Fe K-edge XANES analysis was carried out during the catalyst reduction using 4 cm³·min⁻¹ of H_2 and 80.1 cm³·min⁻¹ of Ar, heating from 323 K to 923 K (10 K·min⁻¹), and subsequently holding this temperature for 2 h. Iron foil was used to calibrate the Fe K-edge absorption peak at 7112 eV. Linear combination analysis was performed using the Athena software [36]. Iron foil, FeO, Fe_3O_4, and hematite (Fe_2O_3) were used as references.

2.3. Catalytic tests

NH_3 decomposition was conducted as a test reaction in order to probe the promoter effects and the thermal stability of the reduced catalysts. The NH_3 decomposition experiments were carried out in a quartz U-tube reactor. A mixture of 10 mg of catalyst and 100 mg of silicon carbide (SiC) was packed between quartz wool plugs. Before the catalytic test, the catalyst was purged using 25 cm³·min⁻¹ of helium (He) for 30 min at room temperature; next, it was reduced using 25 cm³·min⁻¹ of H_2 at 673 K with a heating rate of 5 K·min⁻¹ for 1 h. The reactor was cooled to 323 K under 25 cm³·min⁻¹ of He to flush out H_2. Subsequently, the reactant gases (5 cm³·min⁻¹ of 10% NH_3 in He and 45 cm³·min⁻¹ of He) were fed to the reactor for approximately 20 min to obtain constant flow conditions. The reactor was then heated to 923 K with a 5 K·min⁻¹ heating rate, and this temperature was subsequently held for 1 h. Afterward, the reactor was cooled from 923 K to room temperature with a 5 K·min⁻¹ rate in the same atmosphere. The effluent was connected to a non-dispersive infrared (IR) detector (Rosemount Analytical, NGA 2000) to monitor the NH_3 concentration.

For CO_2 hydrogenation, a mixture of 40 mg of catalyst and 160 mg

of SiC was loaded into the reactor and placed between quartz wool plugs. SiC was used as a diluent to minimize the effect of heat generated by the mildly exothermic reaction. Before the catalytic test, the catalyst was reduced at 653 K and 25 bar (1 bar = 10^5 Pa) under 50 $cm^3 \cdot min^{-1}$ of H_2 for 5 h. The reactor was then cooled to 633 K under 30 $cm^3 \cdot min^{-1}$ of Ar to flush out H_2. The reactant gases (22.5 $cm^3 \cdot min^{-1}$ of H_2, 7.5 $cm^3 \cdot min^{-1}$ of CO_2, and 3.3 $cm^3 \cdot min^{-1}$ of Ar) were passed through the catalyst bed with a gas hourly space velocity (GHSV) of 50 $L \cdot (g \cdot h)^{-1}$ at 633 K and 25 bar. The products were directly measured by an online gas chromatograph (GC) equipped with a thermal conductivity detector (TCD) and two flame ionization detectors (FIDs) using argon as the internal standard. The experimental setup is described in detail elsewhere [37].

3. Results and discussion

Table 1 [32] summarizes the metals' weight percentages in the calcined samples, as analyzed via AAS. The XRD patterns of the unpromoted Fe/NCNT and the promoted Fe/NCNT samples after calcination revealed the presence of Fe_3O_4 as a major iron phase in all catalysts, in addition to hexagonal graphite [32].

Fig. 1 shows the TPR profiles of the calcined Fe/NCNT, K/Fe/NCNT, Mn/Fe/NCNT, and K/Mn/Fe/NCNT catalysts. For the unpromoted iron oxide nanoparticles on NCNTs (Fig. 1(a)), two small peaks were observed at 584 K and 613 K, which can be attributed to the reduction of oxidic iron surface species and the reduction of Fe_2O_3 to Fe_3O_4, respectively [2]. The peak at 773 K can be assigned to the further reduction of Fe_3O_4 to metallic iron. The TPR profiles showed a stepwise reduction of the iron oxide nanoparticles, according to Eq. (3) [5,38].

$$Fe_2O_3 \longrightarrow Fe_3O_4 \longrightarrow Fe \qquad (3)$$
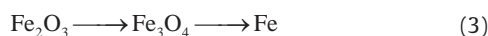
The TPR profile of K/Fe/NCNT shifted to a higher temperature (598 K, 636 K, and 792 K) (Fig. 1(b)), indicating that the reducibility of the Fe catalyst was retarded by the addition of potassium [30]. The onset of the reduction temperatures of the Mn-promoted Fe catalysts (Mn/Fe/NCNT and K/Mn/Fe/NCNT) shifted to a lower temperature, from 485 K to 420 K (Fig. 1(c) and Fig. 1(d)), compared with the unpromoted and K-promoted Fe catalysts, and there was no small peak due to the surface iron oxide. This observation indicates that the iron oxide nanoparticles present in the Mn-promoted samples were more easily reduced than those on the Mn-free samples, which could result from a higher dispersion of iron oxide, corresponding to the results of Tao et al. [20]. For Mn/Fe/NCNT, the peak at low temperature (615 K) corresponded to the reduction of Fe_2O_3 to Fe_3O_4, and the double peaks at high temperature (753 K and 821 K) originated from the further reduction of Fe_3O_4 to Fe (Fig. 1(c)). This reduction appeared as two peaks, which could be attributed to the reduction of Fe_3O_4 to FeO as an intermediate, followed by further reduction to Fe, rather than a one-step reduction at 773 K. The presence of Mn led to the incorporation of Mn^{2+} into the FeO lattice, stabilizing the FeO phase as an intermediate [20]. Similar to Mn/Fe/NCNT, two separate peaks at high temperature (744 K and 807 K) were observed for K/Mn/Fe/NCNT (Fig. 1(d)), and the reduction temperatures of $Fe_3O_4 \rightarrow FeO \rightarrow Fe$ were lower. It can be stated that FeO

was less stable when K was incorporated. Pernicone et al. [39] found that FeO was more easily reducible and showed higher activity in NH_3 synthesis than conventional Fe_3O_4-based catalysts. Thus, in the Mn-promoted Fe/NCNT catalyst (Mn/Fe/NCNT), the FeO intermediate seems to be present during the reduction, favoring the formation of metallic Fe nanoparticles. When Fe/NCNT was promoted with both K and Mn, the FeO intermediate was reduced more easily to the metallic Fe nanoparticles.

In situ XANES experiments were performed in order to better understand the structural evolution of the Fe catalysts, that is, Fe/NCNT, K/Fe/NCNT, Mn/Fe/NCNT, and K/Mn/Fe/NCNT, during the reduction in H_2 prior to CO_2 hydrogenation. Fig. 2 presents stacks of Fe K-edge XANES spectra collected during heating from 323 K to 923 K in H_2 for all four catalysts. The XANES spectra evolved gradually with temperature in all samples. Several steps of phase transformation were monitored as changes of XANES features; the absorption edge shifted toward lower energies, and the white line became depleted, leading to a spectrum similar to that of metallic iron. A linear combination-fitting (LCF) analysis was subsequently employed to deduce the evolution of phase composition during the reduction of the Fe catalysts, as illustrated in Fig. 3. In all cases, the evolution of XANES spectra revealed three steps of phase transformations— hematite (Fe_2O_3) → magnetite (Fe_3O_4) → wüstite (FeO) → metallic iron (Fe)—but with different reaction rates and phase fractions. These results are consistent with our previous study that was performed on non-promoted Fe catalysts [2]. At the beginning of the reaction, most of the calcined precursors consisted of a mixture of the hematite and magnetite phases, except for K/Fe/NCNT, which was mainly composed of hematite. The reduction of hematite to magnetite started at around 473 K, 473 K, 613 K, and 523 K for Fe/NCNT, K/Fe/NCNT, Mn/Fe/NCNT, and K/Mn/Fe/NCNT, respectively. This phase transformation occurred progressively until the hematite fully transformed into magnetite at about 593 k and 623 K for the K-promoted catalysts K/Fe/NCNT and K/Mn/Fe/NCNT, respectively. In contrast, a coexistence of magnetite and wüstite was found at the depletion of hematite at about 513 K and 773 K for Fe/NCNT and
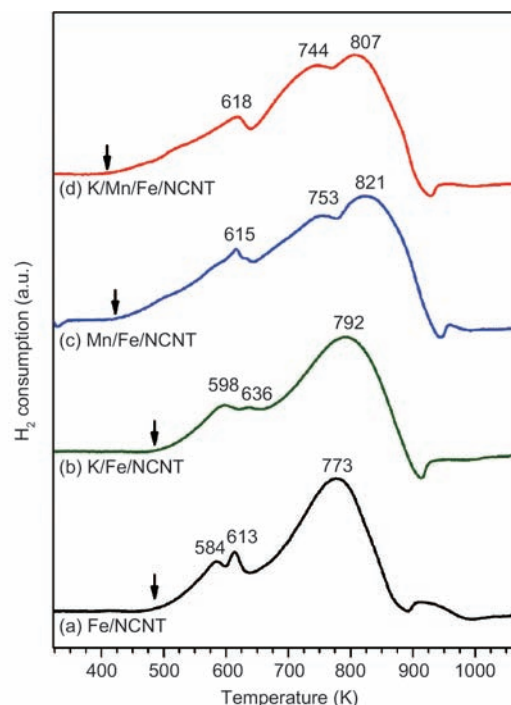
Table 1
Composition of metals in the catalysts [32].

Sample	Weight content (%)		
	Fe	K	Mn
Fe/NCNT	34.2	—	—
K/Fe/NCNT	31.2	1.3	—
Mn/Fe/NCNT	32.8	—	7.1
K/Mn/Fe/NCNT	22.5	1.0	5.4

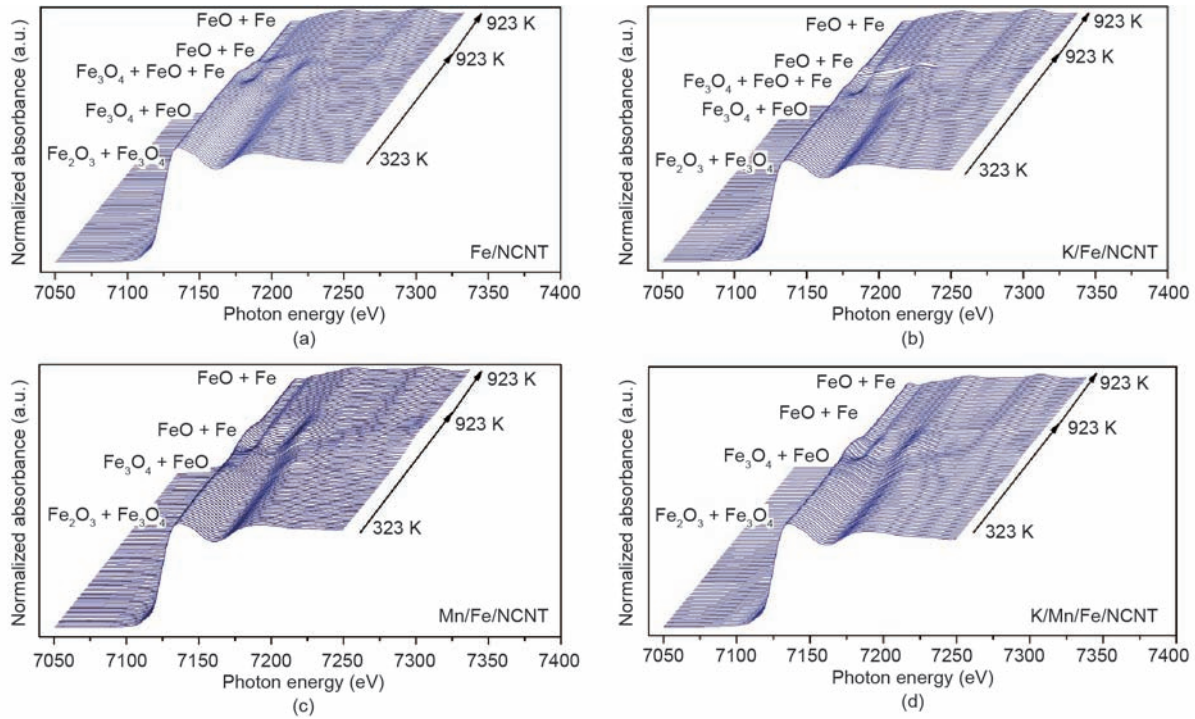**Fig. 1.** H_2-TPR profiles of the calcined (a) Fe/NCNT, (b) K/Fe/NCNT, (c) Mn/Fe/NCNT, and (d) K/Mn/Fe/NCNT precursors before reaction.

Fig. 2. XANES spectra of (a) Fe/NCNT, (b) K/Fe/NCNT, (c) Mn/Fe/NCNT, and (d) K/Mn/Fe/NCNT during heating from 323 K to 923 K (10 K·min⁻¹) using a flow rate of 4 cm³·min⁻¹ of H₂ and 80.1 cm³·min⁻¹ of Ar.
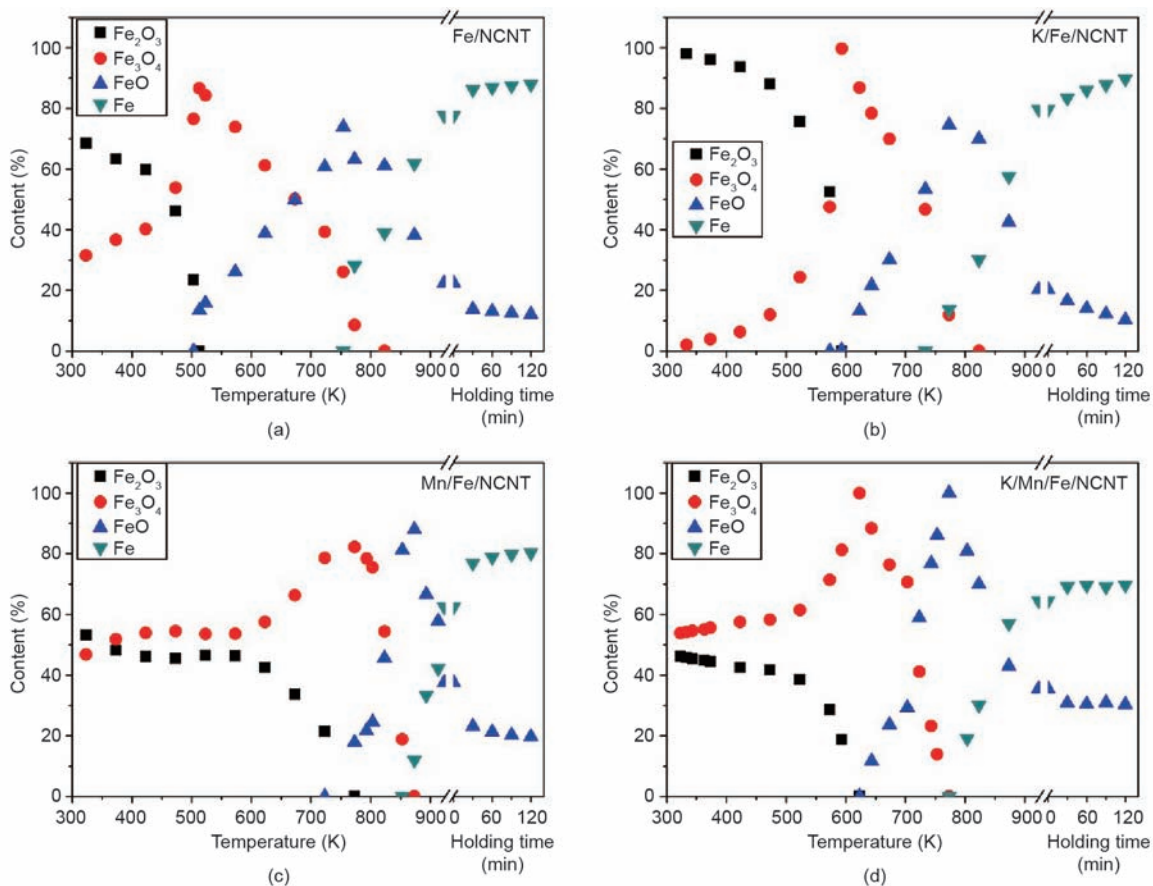
Fig. 3. Phase evolution of the Fe catalysts under *in situ* XANES reduction conditions: 4 cm³·min⁻¹ of H₂ and 80.1 cm³·min⁻¹ of Ar, heating from 323 K to 923 K with a heating rate of 10 K·min⁻¹ and holding for 2 h as a function of temperature. (a) Fe/NCNT; (b) K/Fe/NCNT; (c) Mn/Fe/NCNT; (d) K/Mn/Fe/NCNT.

Mn/Fe/NCNT, respectively. Magnetite was then gradually reduced into wüstite before becoming metallic iron. It is interesting to note that in the Mn-promoted catalysts Mn/Fe/NCNT and K/Mn/Fe/NCNT, the magnetite almost completely transformed into wüstite (ca. 88% and 100% wüstite) before the appearance of metallic iron, whereas this behavior was less pronounced for other catalysts. Finally, the formation of metallic iron in the Fe/NCNT, K/Fe/NCNT, Mn/Fe/NCNT, and K/Mn/Fe/NCNT catalysts took place above 773 K, 773 K, 873 K, and 803 K, respectively. After heating at 923 K for 2 h, metallic iron was obtained as the major phase with a small contribution of wüstite for all samples.

NH_3 decomposition was performed as a test reaction to characterize the promoter effects on the thermal stability of the reduced catalysts. Fig. 4 shows the degree of NH_3 conversion as a function of temperature over unpromoted and promoted iron supported on NCNTs. NH_3 did not decompose on heating up to 923 K during the blank experiment, excluding thermal decomposition at temperatures below 923 K in all the experiments. The onset temperatures for NH_3 decomposition were almost the same for all the catalysts, at about 530 K. The degree of NH_3 conversion over Fe/NCNT increased during heating and reached about 98% at 923 K, indicating that Fe nanoparticles supported on NCNTs were active for NH_3 decomposition. The conversion of NH_3 decreased from 98% to 87% during holding at 923 K for 1 h, indicating deactivation of the catalyst. NH_3 adsorbs on an empty site of the metallic iron surface, followed by sequential NH_3 decomposition [40]:

$$NH_3—^* + ^* \longrightarrow NH_2—^* + H—^* \tag{4}$$

$$NH_2—^* + ^* \longrightarrow NH—^* + H—^* \tag{5}$$

$$NH—^* + ^* \longrightarrow N—^* + H—^* \tag{6}$$

$$2N—^* + ^* \longrightarrow N_2 + 2^* \tag{7}$$
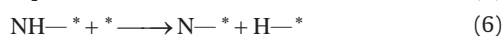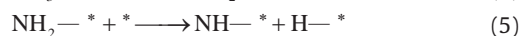
where * represents an empty site on the metallic iron surface.

For K/Fe/NCNT, the onset of NH_3 decomposition was 583 K, which is slightly lower than the onset that was observed for Fe/NCNT. It has been reported that the recombinative desorption step of adsorbed atomic nitrogen (Eq. (7)) is the rate-determining step of NH_3 decomposition [30]. The K promoter destabilizes N—* species, leading to higher activity of NH_3 decomposition over K/Fe/NCNT. In addition, Jedynak et al. [41] found that the K-promoted Fe catalyst exhibited a higher dispersion of Fe nanoparticles. However, the conversion of NH_3 decreased at about 840 K, presumably due to the sintering of the Fe nanoparticles. Deactivation was significant for K/Fe/NCNT,
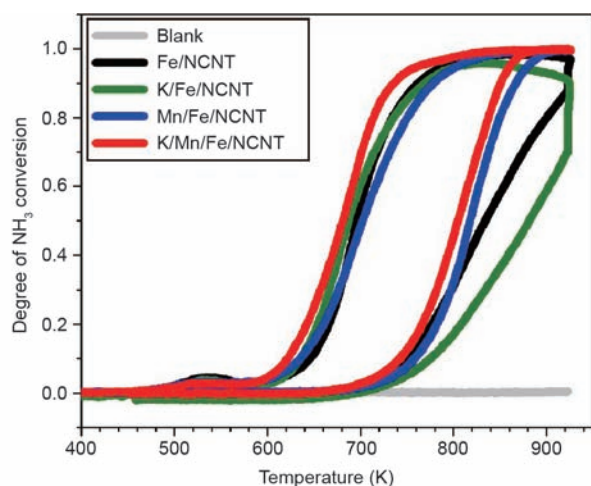
which decomposed NH_3 at around 70% during holding at 923 K for 1 h.

In contrast to Fe/NCNT and K/Fe/NCNT, NH_3 conversion over Mn/Fe/NCNT reached the highest degree and was almost constant at 99% during holding at 923 K, indicating that Mn stabilized the metallic Fe nanoparticles. K/Mn/Fe/NCNT showed the best performance in NH_3 decomposition, reaching the highest degree at 760 K and remaining constant during the holding period. It can thus be suggested that K performed as an electronic promoter and destabilized the N—* species, leading to higher activity in NH_3 decomposition, whereas Mn performed as a structural promoter, preventing severe sintering.

When the catalysts were cooled down, the degree of NH_3 conversion in the cooling cycle was lower than in the heating cycle, because the catalytic activity of the catalysts deteriorated at 923 K. Correspondingly, hysteresis was observed for all four catalysts. K/Mn/Fe/NCNT still showed the best performance, reaching the highest degree of NH_3 conversion. The catalytic activities of the deactivated catalysts are as follows: K/Mn/Fe/NCNT still reached 99% conversion at 860 K, whereas Mn/Fe/NCNT converted NH_3 by 90% and K/Fe/NCNT by 45%, compared with 65% for the unpromoted Fe/NCNT. Obviously, the Mn promoter enhanced the dispersion of the Fe nanoparticles and prevented their sintering [42].

All catalysts were applied in CO_2 hydrogenation at 633 K and 25 bar for 60 h. After the reaction, the catalysts were characterized by XRD, resulting in the patterns shown in Fig. 5. For the Fe/NCNT catalyst (Fig. 5(a)), the diffraction peaks at 40.9°, 43.5°, and 44.2° originate from Hägg carbide (χ-Fe_5C_2), whereas the diffraction peaks at 30.4° and 35.8° are due to magnetite. During CO_2 hydrogenation, the reduced iron phase was transformed into iron carbide, which is catalytically active for the FTS reaction, whereas water produced by the FTS reaction partly oxidized the iron to magnetite. On the other hand, the K/Fe/NCNT catalyst (Fig. 5(b)) exhibited χ-Fe_5C_2 as the major iron phase even after the long reaction time of 60 h. The diffraction patterns of Mn/Fe/NCNT (Fig. 5(c)) showed diffraction peaks at 40.9°, 43.5°, and 44.2°, which correspond to χ-Fe_5C_2, and peaks at 24.3°, 31.4°, and 51.8°, which correspond to manganese carbonate ($MnCO_3$). The $MnCO_3$ peaks were clearly observed for the K/Mn/Fe/NCNT catalyst (Fig. 5(d)). Grzybek et al. [43] studied Mn/Fe oxide catalysts and found that the catalyst surface was enriched in Mn, which may inhibit the oxidation of iron to magnetite [43]. Mn is also able to retard the agglomeration of iron oxide nanoparticles, which are formed during the reaction [42]. After 60 h reaction time, K/Mn/Fe/NCNT still exposed the XRD pattern of the active χ-Fe_5C_2 phase without detectable magnetite reflections.

Fig. 4. Degree of NH_3 conversion as a function of temperature over unpromoted and promoted Fe nanoparticles supported on NCNTs.
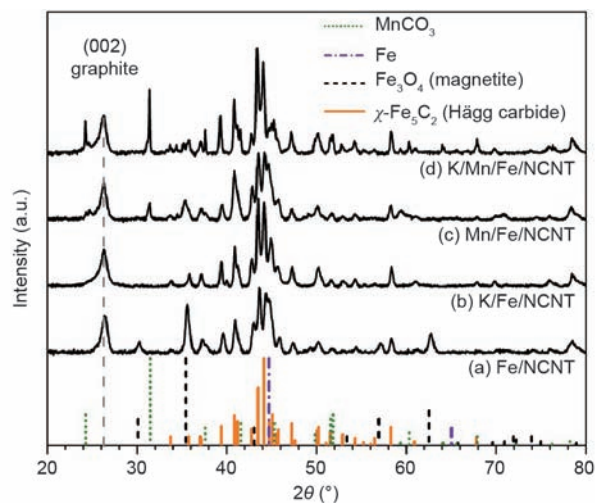

Fig. 5. XRD patterns of (a) Fe/NCNT, (b) K/Fe/NCNT, (c) Mn/Fe/NCNT, and (d) K/Mn/Fe/NCNT after CO_2 hydrogenation at 633 K and 25 bar for 60 h.

Fig. 6(a) shows the CO_2 conversion over Fe/NCNT, K/Fe/NCNT, Mn/Fe/NCNT, and K/Mn/Fe/NCNT as a function of time on stream at 633 K. The reaction over Fe/NCNT had a degree of CO_2 conversion of about 38% at the beginning, and the activity continuously decreased with time on stream. The deactivation of the catalyst points to sintering of the Fe nanoparticles at high temperature over the long reaction time. The Mn-promoted Fe catalyst (Mn/Fe/NCNT) showed a lower conversion at the beginning of around 30%, but it was more constant than the unpromoted Fe catalyst. Grzybek et al. [43] found that the surface of the catalyst was enriched with Mn and was larger after reduction. It is assumed that an outer surface enriched in Mn shields the active Fe from the reaction [42], but carbon atoms were still able to diffuse through the Mn-rich surface to form iron carbide that was available for the hydrogenation reaction [43]. Thus, the Mn promoter is a structural promoter that stabilizes the active iron phase, as indicated by the H_2-TPR and NH_3 decomposition experiments, resulting in stable catalytic activity for CO_2 hydrogenation during the 60 h on stream. Both K-promoted catalysts exhibited

high CO_2 conversion of over 30%. The doubly promoted iron catalyst K/Mn/Fe/NCNT showed a slightly lower conversion of about 30%, but more constant CO_2 hydrogenation performance. It is clear that K promotes CO_2 hydrogenation and Mn enhances the structural stability of the active iron carbide nanoparticles.

Fig. 6(b) and Table 2 show the product selectivities over Fe/NCNT, K/Fe/NCNT, Mn/Fe/NCNT, and K/Mn/Fe/NCNT. All the catalysts produced mainly CO, a result that was in agreement with the findings of Lee et al. [44]. Wang et al. [1] also reported that K acts as a promoter for CO_2 adsorption, creating new active sites for decomposition to CO. It has also been reported that the FTS reaction rate is much slower than that of the RWGS reaction [43], which results in the suppression of methane formation and high selectivity for long-chain hydrocarbons. The product selectivity over Mn-promoted Fe/NCNT was somewhat similar to that of the unpromoted Fe/NCNT. In addition, the formation of oxygenated hydrocarbons over Mn/Fe/NCNT was not observed.

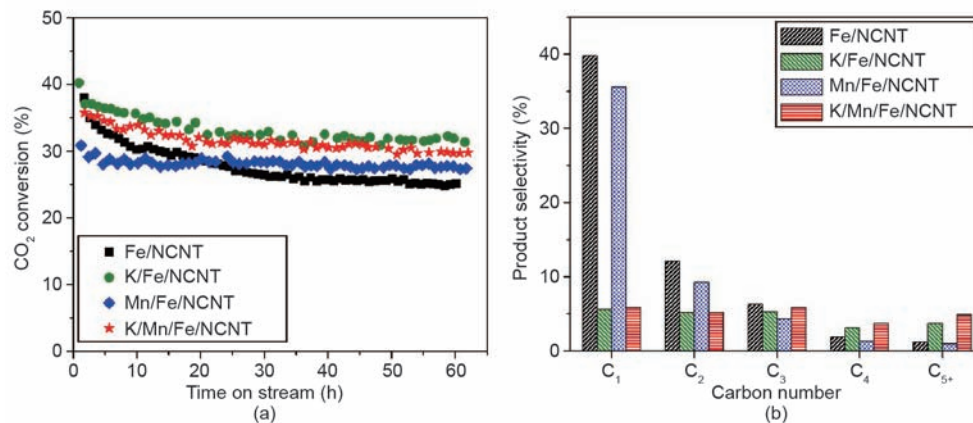To investigate the catalytic performance of K/Mn/Fe/NCNT in

Fig. 6. (a) CO_2 conversion as a function of time on stream and (b) product selectivities.

Table 2
Product selectivities, olefin selectivities in the C_2–C_5 range, chain-growth probabilities (α), and CO_2 conversion (X_{CO_2}) over the iron catalysts after 60 h time on stream.

Catalyst	Product selectivity (%)							$C_{2=}$–$C_{5=}$/C_2–C_5	α	X_{CO_2} (%)
	CO	C_1	C_2	C_3	C_4	C_{5+}	Alcohol			
Fe/NCNT	38.4	39.8	12.1	6.3	1.9	1.2	0.2	0.09	0.29	25.4
K/Fe/NCNT	74.6	5.6	5.2	5.3	3.1	3.7	2.0	0.87	0.44	31.8
Mn/Fe/NCNT	48.5	35.6	9.3	4.3	1.3	1.0	0.1	0.11	0.34	27.6
K/Mn/Fe/NCNT	72.1	5.9	5.2	5.9	3.7	4.9	2.4	0.89	0.45	30.1

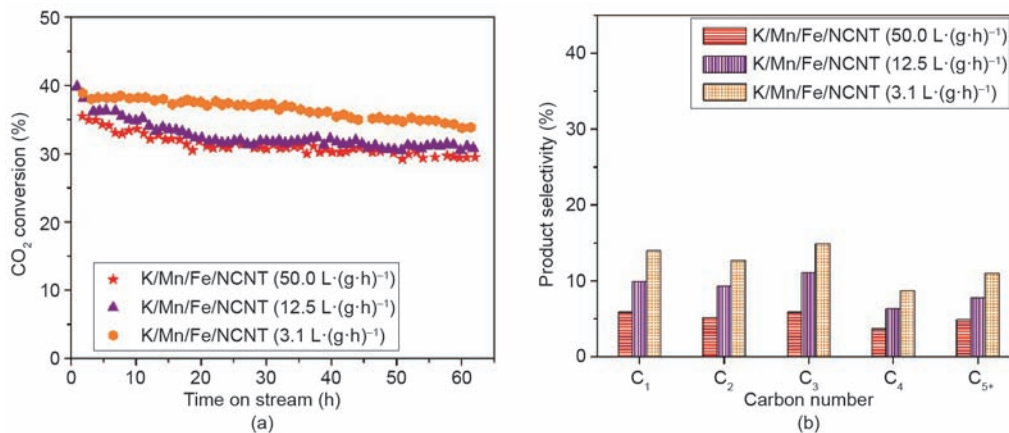Reaction conditions: 633 K, 25 bar, GHSV of 50 L·(g·h)$^{-1}$.

Fig. 7. (a) CO_2 conversion as a function of time on stream and (b) product selectivities resulting from CO_2 hydrogenation over K/Mn/Fe/NCNT with different residence times.

Table 3
Product distribution over K/Mn/Fe/NCNT after 60 h time on stream.

Catalyst	Product selectivity (%)							$C_{2=}-C_{5=}/C_2-C_5$	α	X_{CO_2} (%)
	CO	C_1	C_2	C_3	C_4	C_{5+}	Alcohol			
K/Mn/Fe/NCNT[a]	72.1	5.9	5.2	5.9	3.7	4.9	2.4	0.89	0.45	30.1
K/Mn/Fe/NCNT[b]	50.5	9.9	9.3	11.1	6.4	7.8	4.9	0.90	0.45	31.0
K/Mn/Fe/NCNT[c]	29.5	14.0	12.7	14.9	8.7	11.0	8.4	0.90	0.47	34.9

[a] The catalyst mass is 40 mg and the GHSV is 50.0 L·(g·h)$^{-1}$.
[b] The catalyst mass is 160 mg and the GHSV is 12.5 L·(g·h)$^{-1}$.
[c] The catalyst mass is 640 mg and the GHSV is 3.1 L·(g·h)$^{-1}$.

more detail, the residence time in the reaction zone was increased by increasing the catalyst weight. Fig. 7 and Table 3 show higher CO_2 conversion and hydrocarbon selectivities, with lower CO selectivity and high olefin and alcohol selectivities.

High olefin selectivities and alcohols produced from CO_2 hydrogenation were obtained with K-promoted catalysts. In the FTS mechanism for the formation of hydrocarbons, adsorbed CO on the active Fe species is reduced to $CH_2—*$ and then forms $CH_3—CH_2—*$. If the surface of the catalyst is polar, as in the presence of K^+, it can abstract hydride ions from adsorbed ethyl species, producing $CH_2=CH_2$ as a product. Thus, both K-promoted catalysts produced high olefin contents, although K/Fe/NCNT was easily sintered, causing unstable activity during the long reaction time. The K-promoted catalyst seemed to adsorb H_2O, thus favoring the partial oxidation of $—CH_2—$ species to alcohols, and the doubly promoted K/Mn/Fe/NCNT with Mn as an additional structural promoter showed a more constant performance. Further studies are in progress, aiming at optimization of the amounts of K and Mn promoters. These studies will include sulfur as an additional promoter because it is known to be highly effective when combined with sodium.

4. Conclusions

The influence of the promoters K and Mn on Fe nanoparticles (K/Mn/Fe/NCNT) supported on NCNTs was studied during CO_2 hydrogenation at 25 bar. In all the calcined catalysts, Fe_3O_4 was mainly present; it then transformed into χ-Fe_5C_2 during CO_2 hydrogenation. After the reaction with the doubly promoted catalyst K/Mn/Fe/NCNT, the active χ-Fe_5C_2 phase was the dominant iron phase, with some additional $MnCO_3$. The K promoter lowered the reducibility of the catalysts, as shown by the H_2-TPR and *in situ* XANES analysis. The Mn promoter stabilized FeO as an intermediate and lowered the H_2-TPR onset temperature. NH_3 decomposition was used as a probe reaction, showing that the doubly promoted catalyst K/Mn/Fe/NCNT achieved the highest catalytic activity and thermal stability. The doubly promoted catalyst K/Mn/Fe/NCNT also showed the best FTS performance, resulting in high CO_2 conversion, low selectivities for hydrocarbons, and high selectivities for short-chain olefins. A high CO_2 conversion of 34.9% with a high alkene/alkane ratio and a low CO selectivity of 29.5% were achieved when using a GHSV of 3.1 L·(g·h)$^{-1}$. All catalytic results clearly show that K acts as an electronic promoter, modifying the surface chemistry of the Fe nanoparticles, whereas Mn acts as a structural promoter, stabilizing them against sintering.

Compliance with ethics guidelines

Praewpilin Kangvansura, Ly May Chew, Chanapa Kongmak, Phatchada Santawaja, Holger Ruland, Wei Xia, Hans Schulz, Attera Worayingyong, and Martin Muhler declare that they have no conflict of interest or financial conflicts to disclose.

References

[1] Wang W, Wang S, Ma X, Gong J. Recent advances in catalytic hydrogenation of carbon dioxide. Chem Soc Rev 2011;40(7):3703–27.
[2] Chew LM, Kangvansura P, Ruland H, Schulte HJ, Somsen C, Xia W, et al. Effect of nitrogen doping on the reducibility, activity and selectivity of carbon nanotube-supported iron catalysts applied in CO_2 hydrogenation. Appl Catal A Gen 2014;482:163–70.
[3] Schulz H, Riedel T, Schaub G. Fischer-Tropsch principles of co-hydrogenation on iron catalysts. Top Catal 2005;32:117–24.
[4] Schulz H. Comparing Fischer-Tropsch synthesis on iron- and cobalt catalysts: The dynamics of structure and function. Stud Surf Sci Catal 2007;163:177–99.
[5] Abbaslou RMM, Tavassoli A, Soltan J, Dalai AK. Iron catalysts supported on carbon nanotubes for Fischer-Tropsch synthesis: Effect of catalytic site position. Appl Catal A Gen 2009;367(1–2):47–52.
[6] Riedel T, Schulz H, Schaub G, Jun KW, Hwang JS, Lee KW. Fischer-Tropsch on iron with H_2/CO and H_2/CO_2 as synthesis gases: The episodes of formation of the Fischer-Tropsch regime and construction of the catalyst. Top Catal 2003;26(1):41–54.
[7] Riedel T, Claeys M, Schulz H, Schaub G, Nam SS, Jun KW, et al. Comparative study of Fischer-Tropsch synthesis with H_2/CO and H_2/CO_2 syngas using Fe- and Co-based catalysts. Appl Catal A Gen 1999;186(1–2):201–13.
[8] Srinivas S, Malik RK, Mahajani SM. Fischer-Tropsch synthesis using bio-syngas and CO_2. Energy Sustain Dev 2007;11(4):66–71.
[9] Chen W, Fan Z, Pan X, Bao X. Effect of confinement in carbon nanotubes on the activity of Fischer-Tropsch iron catalyst. J Am Chem Soc 2008;130(29):9414–9..
[10] de Smit E, Beale AM, Nikitenko S, Weckhuysen BM. Local and long range order in promoted iron-based Fischer-Tropsch catalysts: A combined *in situ* X-ray absorption spectroscopy/wide angle X-ray scattering study. J Catal 2009;262:244–56.
[11] Pour AN, Housaindokht MR, Tayyari SF, Zarkesh J. Fischer-Tropsch synthesis by nano-structured iron catalyst. J Nat Gas Chem 2010;19(3):284–92.
[12] Pour AN, Housaindokht MR, Tayyari SF, Zarkesh J. Deactivation studies of nano-structured iron catalyst in Fischer-Tropsch synthesis. J Nat Gas Chem 2010;19(3):333–40.
[13] de Smit E, Cinquini F, Beale AM, Safonova OV, van Beek W, Sautet P, et al. Stability and reactivity of ε-χ-θ iron carbide catalyst phases in Fischer-Tropsch synthesis: Controlling μ_c. J Am Chem Soc 2010;132(42):14928–41.
[14] Xiong H, Moyo M, Motchelaho MA, Jewell LL, Coville NJ. Fischer-Tropsch synthesis over model iron catalysts supported on carbon spheres: The effect of iron precursor, support pretreatment, catalyst preparation method and promoters. Appl Catal A Gen 2010;388(1–2):168–78.
[15] Yu G, Sun B, Pei Y, Xie S, Yan S, Qiao M, et al. Fe_xO_y@C spheres as an excellent catalyst for Fischer-Tropsch synthesis. J Am Chem Soc 2010;132(3):935–7.
[16] Dorner RW, Hardy DR, Williams FW, Willauer HD. Heterogeneous catalytic CO_2 conversion to value-added hydrocarbons. Energy Environ Sci 2010;3(7):884–90.
[17] Dorner RW, Hardy DR, Williams FW, Willauer HD. K and Mn doped iron-based CO_2 hydrogenation catalysts: Detection of $KAlH_4$ as part of the catalyst's active phase. Appl Catal A Gen 2010;373(1–2):112–21.
[18] Bahome MC, Jewell LL, Hildebrandt D, Glasser D, Coville NJ. Fischer-Tropsch synthesis over iron catalysts supported on carbon nanotubes. Appl Catal A Gen 2005;287(1):60–7.
[19] Ribeiro MC, Jacobs G, Davis BH, Cronauer DC, Kropf AJ, Marshall CL. Fischer-Tropsch synthesis: An *in situ* TPR-EXAFS/XANES investigation of the influence of group I alkali promoters on the local atomic and electronic structure of carburized iron/silica catalysts. J Phys Chem C 2010;114(17):7895–903.
[20] Tao Z, Yang Y, Wan H, Li T, An X, Xiang H, et al. Effect of manganese on a potassium-promoted iron-based Fischer-Tropsch synthesis catalyst. Catal Lett 2007;

114(3):161–8.

[21] Campos A, Lohitharn N, Roy A, Lotero E, Goodwin JG, Spivey JJ. An activity and XANES study of Mn-promoted, Fe-based Fischer-Tropsch catalysts. Appl Catal A Gen 2010;375(1):12–6.

[22] Ribeiro MC, Jacobs G, Pendyala R, Davis BH, Cronauer DC, Kropf AJ, et al. Fischer-Tropsch synthesis: Influence of Mn on the carburization rates and activities of Fe-based catalysts by TPR-EXAFS/XANES and catalyst testing. J Phys Chem C 2011;115:4783–92.

[23] Davis BH. Fischer-Tropsch synthesis: Reaction mechanisms for iron catalysts. Catal Today 2009;141(1–2):25–33.

[24] Torres Galvis HM, Bitter JH, Khare CB, Ruitenbeek M, Dugulan AI, de Jong KP. Supported iron nanoparticles as catalysts for sustainable production of lower olefins. Science 2012;335(6070):835–8.

[25] Tavasoli A, Sadagiani K, Khorashe F, Seifkordi A, Rohani A, Nakhaeipour A. Cobalt supported on carbon nanotubes—A promising novel Fischer-Tropsch synthesis catalyst. Fuel Process Technol 2008;89(5):491–8.

[26] van Steen E, Prinsloo FF. Comparison of preparation methods for carbon nanotubes supported iron Fischer-Tropsch catalysts. Catal Today 2002;71(3–4):327–34.

[27] Schulte HJ, Graf B, Xia W, Muhler M. Nitrogen- and oxygen-functionalized multiwalled carbon nanotubes used as support in iron-catalyzed, high-temperature Fischer-Tropsch synthesis. ChemCatChem 2012;4(3):350–5.

[28] Dorner RW, Hardy DR, Williams FW, Willauer HD. Catalytic CO_2 hydrogenation to feedstock chemicals for jet fuel synthesis using multi-walled carbon nanotubes as support. In: Hu YH, editor Advances in CO_2 conversion and utilization. Washington DC: American Chemical Society; 2010. p. 125–39.

[29] Kundu S, Xia W, Busser W, Becker M, Schmidt DA, Havenith M, et al. The formation of nitrogen-containing functional groups on carbon nanotube surfaces: A quantitative XPS and TPD study. Phys Chem Chem Phys 2010;12(17):4351–9..

[30] Kowalczyk Z, Sentek J, Jodzis S, Muhler M, Hinrichsen O. Effect of potassium on the kinetics of ammonia synthesis and decomposition over fused iron catalyst at atmospheric pressure. J Catal 1997;169(2):407–14.

[31] Arabczyk W, Zamlynny J. Study of the ammonia decomposition over iron catalysts. Catal Lett 1999;60(3):167–71.

[32] Kangvansura P, Chew LM, Saengsui W, Santawaja P, Poo-arporn Y, Muhler M, et al. Product distribution of CO_2 hydrogenation by K- and Mn-promoted Fe catalysts supported on N-functionalized carbon nanotubes. Catal Today

[33] Xia W, Jin C, Kundu S, Muhler M. A highly efficient gas-phase route for the oxygen functionalization of carbon nanotubes based on nitric acid vapor. Carbon 2009;47(3):919–22.

[34] Boot LA, van Dillen AJ, Geus JW, van Buren FR. Iron-based dehydrogenation catalysts supported on zirconia. I. Preparation and characterization. J Catal 1996;163(1):186–94.

[35] Poo-arporn Y, Chirawatkul P, Saengsui W, Chotiwan S, Kityakarn S, Klinkhieo S, et al. Time-resolved XAS (Bonn-SUT-SLRI) beamline at SLRI. J Synchrotron Radiat 2012;19(6):937–43.

[36] Ravel B, Newville M. ATHENA, ARTEMIS, HEPHAESTUS: Data analysis for X-ray absorption spectroscopy using IFEFFIT. J Synchrotron Radiat 2005;12(4):537–41.

[37] Chew LM, Ruland H, Schulte HJ, Xia W, Muhler M. CO_2 hydrogenation to hydrocarbons over iron nanoparticles supported on oxygen-functionalized carbon nanotubes. J Chem Sci 2014;126(2):481–6.

[38] Wimmers OJ, Arnoldy P, Moulijn JA. Determination of the reduction mechanism by temperature-programmed reduction: Application to small iron oxide (Fe_2O_3) particles. J Phys Chem C 1986;90(7):1331–7.

[39] Pernicone N, Ferrero F, Rossetti I, Forni L, Canton P, Riello P, et al. Wüstite as a new precursor of industrial ammonia synthesis catalysts. Appl Catal A Gen 2003;251(1):121–9.

[40] Yeo SC, Han SS, Lee HM. Mechanistic investigation of the catalytic decomposition of ammonia (NH_3) on an Fe(100) surface: A DFT study. J Phys Chem C 2014;118(10):5309–16.

[41] Jedynak A, Kowalczyk Z, Szmigiel D, Rarog W, Zielinski J. Ammonia decomposition over the carbon-based iron catalyst promoted with potassium. Appl Catal A Gen 2002;237(1–2):223–6.

[42] Dad M, Fredriksson H, van de Loosdrecht J, Thuene P, Niemantsverdriet J. Stabilization of iron by manganese promoters in uniform bimetallic FeMn Fischer-Tropsch model catalysts prepared from colloidal nanoparticles. Catal Struct React 2015;1(2):101–9.

[43] Grzybek T, Klinik J, Papp H, Baerns M. Characterization of Cu and K containing Fe/Mn oxide catalysts for Fischer-Tropsch synthesis. Chem Eng Technol 1990;14(1):156–61.

[44] Lee JF, Chern WS, Lee MD. Hydrogenation of carbon dioxide on iron catalysts doubly promoted with manganese and potassium. Can J Chem Eng 1992;70(3):511–5.